ACS Catalysis

Research Article

pubs.acs.org/acscatalysis

Understanding the Role of Metal-Modified Mo(110) Bimetallic Surfaces for C−O/C═O and C−C Bond Scission in C3 Oxygenates

MyatNoeZin Myint[†] and Jingguang G. Chen*[,‡]

[†]Department of Chemical and Biomolecular Engineering, University of Delaware, Newark, Delaware 19716, United States

[‡]Department of Chemical Engineering, Columbia University, New York, New York 10027, United States

Supporting Information

ABSTRACT: Bond scission of C−O/C═O, C−C, and C−H from oxygenates on Mo(110), Ni/Mo(110), and Co/Mo(110) has been investigated via density functional theory (DFT) calculations, temperature-programmed desorption (TPD), and high-resolution electron energy loss spectroscopy (HREELS). Propanal and 1-propanol are used as probe molecules for biomass-derived oxygenates due to their relatively high vapor pressures, allowing their easy introduction into UHV systems. DFT results predict that the binding energy trend of propanal and 1-propanol is Mo(110) > Co/Mo(110) > Ni/Mo(110), which suggests that binding energies are reduced by the modification of Mo(110) with Ni and Co admetals. TPD and HREELS results show that bond scission activity and selectivity can be tuned upon admetal modification of Mo(110). For both molecules, Mo(110) shows a highly selective deoxygenation pathway toward C−O/C═O bond scission to produce propene, while bimetallic surfaces instead exhibit a higher activity for C−C and C−H bond scission. Among the three surfaces, Ni modification leads to the highest selectivity for decarbonylation to produce ethylene and Co modification results in the highest selectivity for reforming to produce syngas.

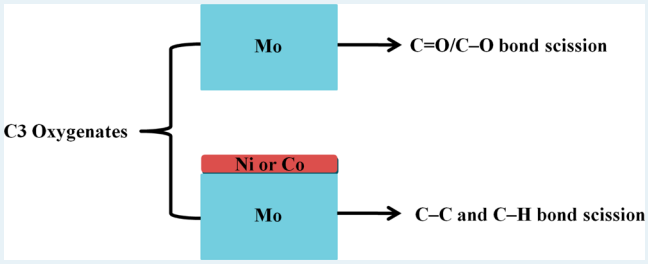

KEYWORDS: *propanal, 1-propanol, deoxygenation, reforming, decarbonylation, nonprecious bimetallic surfaces*

1. INTRODUCTION

The reactions of biomass-derived oxygenates on transition-metal surfaces have been of particular interest in the field of heterogeneous catalysis as a promising way to produce value-added fuels and chemicals from renewable sources.[1−3] Catalytic transformation of oxygenates, particularly the most commonly studied alcohols and aldehydes,[4] includes but is not limited to C−O/C═O bond scission to produce alkenes via deoxygenation, and C−C and C−H bond scission to produce syngas (CO and H_2) via reforming reactions. Selective hydrodeoxygenation (HDO)/deoxygenation is one of the pivotal reactions to remove excess oxygen from bio-oils to produce transportation fuels without reducing the carbon chain length.[5−7] The reforming reaction, on the other hand, is an attractive alternative way to produce hydrogen from renewable biomass, instead of the current production method from fossil fuels.[8,9] Typical HDO and reforming catalysts include precious metal based catalysts such as Pt[10] and Pd,[11,12] but the use of such catalysts in large-scale biomass conversion is hindered by high costs and scarcity of precious metals.[13] Cost-effective nonprecious metal catalysts, however, suffer from low activity and rapid deactivation.[14] The search for enhanced catalytic activity of nonprecious metals requires an understanding of reaction pathways of oxygenates on metal surfaces.

Recently, molybdenum carbide (Mo_2C) and oxide (MoO_3) have been reported to show high selectivity toward C−O/C═O bond scission without breaking the C−C bond.[7,15−22] Since bimetallic catalysts often show superior catalytic performance and a unique ability to control the reaction chemistry of oxygenates,[8,9] in this work, we have investigated the reactivity and reaction intermediates of the C3 oxygenates 1-propanol and propanal as probe molecules on Mo(110) and metal-modified Mo(110) surfaces. Nonprecious bimetallic surfaces, Ni/Mo(110) and Co/Mo(110), have been selected, since sulfided $NiMo/Al_2O_3$ and $CoMo/Al_2O_3$ have long been used as conventional petroleum hydrotreating catalysts.[5,6,19]

Characterization of the Ni/Mo(110) and Co/Mo(110) surfaces has been extensively studied via LEED, STM, and AES; the investigations of the growth of Ni[23−26] and Co[26−29] overlayers on Mo(110) show that both Ni and Co grow layer by layer on Mo(110) at room temperature and form 3D islands upon annealing to >600 K. Reactions of alcohols on clean Mo(110) and modified Mo(110) have been largely reported by Friend's group via surface science studies.[30−37] However, the investigation of reactions of aldehydes on Mo(110) is limited; Mei et al. studied the reaction pathways of acetaldehyde via periodic spin-polarized density functional theory (DFT) simulations,[38] and Queeney et al. reported the reaction of formaldehyde on Mo(110) using temperature-programmed reactions and infrared reflectance absorbance spectroscopy.[39]

Received: August 26, 2014
Revised: October 29, 2014
Published: November 24, 2014

To the best of our knowledge, there has been no experimental UHV study of C3 aldehyde on pure Mo(110) and/or metal-modified Mo(110) surfaces.

Hence, in this study, we investigate the reaction of propanal on Mo(110), monolayer (ML) Ni/Mo(110), and ML Co/Mo(110) surfaces and compare it with that of 1-propanol. We first identify the DFT binding energy trends of propanal and 1-propanol on Mo(110) and metal-modified Mo(110) surfaces. Using temperature-programmed desorption (TPD) and high-resolution electron energy loss spectroscopy (HREELS), reaction products and intermediates are identified and possible reaction pathways are proposed. Briefly summarizing our results, the bond scission of C−C, C−O/C═O, and C−H can be controlled via bimetallic surfaces. While Mo(110) is active for breaking both C═O and C−O bonds in propanal and 1-propanol to produce propene, metal-modified bimetallic surfaces show higher reforming activity and produce other C−C and C−H bond scission products. Our results demonstrate the feasibility of controlling reaction pathways of small oxygenates which can be extended for more complex biomass-derived oxygenate platform molecules.

2. THEORETICAL AND EXPERIMENTAL METHODS

2.1. DFT Calculations. All theoretical calculations were performed with the Vienna ab initio simulation package (VASP).[40−42] Calculation procedures have been described in detail previously.[43] Briefly, the PW91 functional within the generalized gradient approximation (GGA) was used to approximate the exchange-correlation energy. The energy cutoff was 396 eV. The model surfaces in all cases consisted of a periodic 3 × 3 unit cell with four layers of metal atoms at the (110) configuration separated by six equivalent layers of vacuum. The Ni/Mo(110) and Co/Mo(110) surfaces were modified by replacing all Mo atoms from the top layer with Ni or Co adatoms which occupied the epitaxial positions. The bottom two layers of the slab were fixed, while the top two layers and the adsorbate were allowed to relax to reach the lowest energy configuration. Spin polarization was corrected accordingly.

Propanal and propionyl were adsorbed via both η^1 (through the O lone pair) and η^2 (through both C and O atoms of the carbonyl groups) configurations on the atop sites of adjacent metal atoms. As the most representative forms, the optimized geometries of propanal and 1-propanol on Mo(110) are shown in parts a and b of Figure 1, respectively. Propanal adsorbs on all surfaces in an η^2 configuration, where the C and O atoms of the carbonyl group both interact with the surface. This is in agreement with a previous report that acetaldehyde adsorbs on Mo(110) via an η^2 configuration.[38] 1-Propanol adsorbs on an atop binding site of all surfaces through the oxygen atom, with the rest of the molecule being directed away from the surface. Binding energies were calculated using the equation

$$BE_{ads/slab} = E_{ads/slab} - E_{slab} - E_{gas}$$

where $E_{ads/slab}$ is the total energy of the slab with adsorbates, E_{slab} is the energy of the slab, and E_{gas} is the energy of the adsorbates in the gas phase. For all calculations, 1/9 ML coverage was used.

2.2. Experimental Section. The experiments were performed in two ultrahigh-vacuum (UHV) chambers, which have been described previously,[43] with a base pressure of 1 × 10^{-10} Torr. The Mo single-crystal sample is a (110) oriented, 1.50 mm thick disk (99.99%) that has a diameter of 12.00 mm.

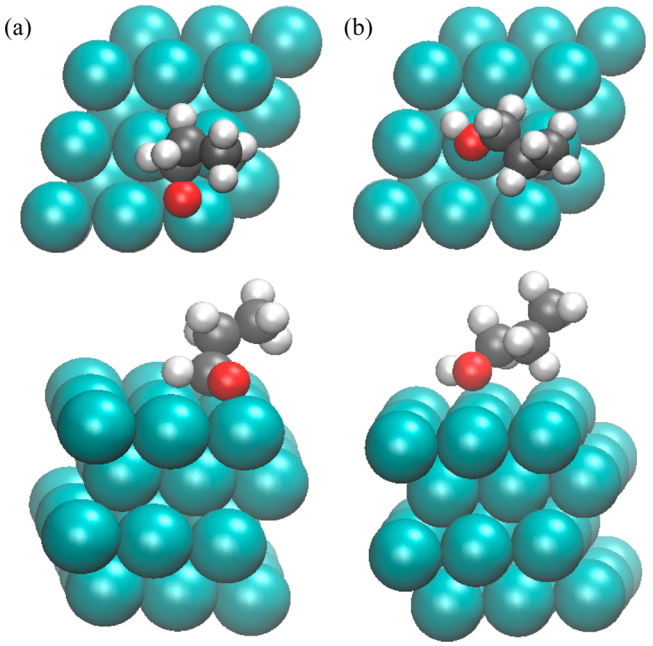

Figure 1. Top and side views of the adsorption geometries of (a) propanal and (b) 1-propanol on Mo(110). Color code: Mo, cyan; C, gray; O, red; H, white.

The crystal was spot-welded directly to two tantalum posts, which served as contacts for heating and cooling. The surface was cleaned by repeated cycles of Ne^+ sputtering at 300 K, followed by annealing at 1100 K. To remove carbon left on the surface, O_2 treatment at 1000 K was performed and the surface was then annealed at 1100 K. This cleaning procedure was repeated until Auger electron spectroscopy (AES) measurements confirmed the absence of C or O on the surface. Bimetallic surfaces were then prepared using previously reported procedures.[43] Briefly, 3*d* metals (Ni, Co) were deposited using physical vapor deposition (PVD). The evaporative PVD doser consisted of a tungsten filament with a high-purity Ni or Co wire (99.9999+% from Alfa Aesar) wrapped around it, mounted within a tantalum enclosure. During deposition, the Mo(110) surface was held at 300 K. The AES ratios of Ni (849 eV)/Mo (190 eV) and Co (777 eV)/Mo(190 eV) were used to determine the Ni and Co monolayer coverages on Mo(110), respectively.

Propanal (Sigma-Aldrich, 97+%) and 1-propanol (Sigma-Aldrich, 99.7+%) were purified via successive freeze−pump−thaw cycles. The purity of all chemicals was checked using mass spectrometry. The surfaces were heated at a linear rate of 3 K/s from 110 to 800 K, and doses are reported in langmuirs (1L = 1 × 10^{-6} Torr s) and are uncorrected for ion gauge sensitivity. All HREELS measurements were performed with a primary beam energy of 6 eV and with the angles of incidence and reflection at 60° with respect to the surface normal.

3. RESULTS

3.1. Adsorbate Binding Energy. The binding energies of propanal, propionyl (CH_3CH_2C═O^*) from the removal of hydrogen through the C−H bond, 1-propanol, and 1-propoxy ($CH_3CH_2CH_2O^*$) obtained after the O−H bond scission on monometallic Mo(110) and metal-modified Mo(110) are summarized in Table 1. Their corresponding optimized C−O bond lengths are shown in Table 2. Overall, the binding energy

dx.doi.org/10.1021/cs5012734 | ACS Catal. 2015, 5, 256−263

Table 1. Binding Energies (kcal/mol) of Adsorbates on Different Surfaces

	propanal (CH_3CH_2CHO)		propionyl ($CH_3CH_2C{=}O^*$)		1-propanol ($CH_3CH_2CH_2OH$)	1-propoxy ($CH_3CH_2CH_2O^*$)
confign	η^1	η^2	η^1	η^2	η^1	η^1
Mo(110)	−29.8	−32.6	−61.1	−72.4	−14.4	−72.5
ML Ni/Mo(110)	−10.1	−15.2	−46.2	−50.1	−10.8	−53.4
ML Co/Mo(110)	−12.9	−23.6	−54.0	−59.7	−11.9	−58.9

Table 2. Optimized C−O Bond Lengths (Å) of Adsorbates on Different Surfaces

	propanal (CH_3CH_2CHO)		propionyl ($CH_3CH_2C{=}O^*$)		1-propanol ($CH_3CH_2CH_2OH$)	1-propoxy ($CH_3CH_2CH_2O^*$)
confign	η^1	η^2	η^1	η^2	η^1	η^1
Mo(110)	1.42	1.42	1.33	1.36	1.46	1.41
ML Ni/Mo(110)	1.24	1.33	1.27	1.30	1.47	1.42
ML Co/Mo(110)	1.25	1.37	1.29	1.33	1.47	1.41

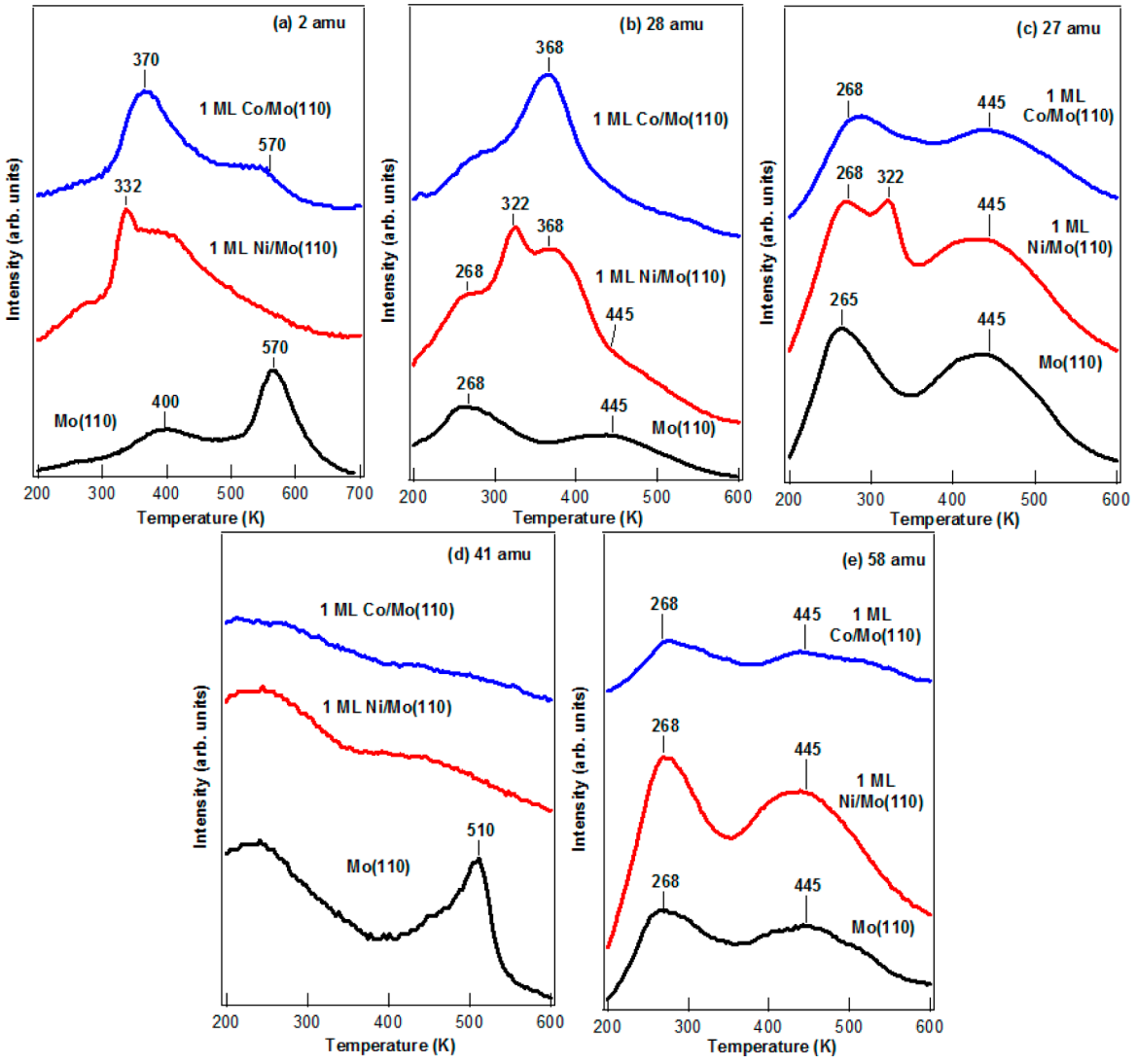

Figure 2. TPD spectra of (a) m/e = 2 (H_2), (b) m/e = 28 (CO, C_2H_4 and propanal), (c) m/e = 27 (C_2H_4 and propanal), (d) m/e = 41 (propene), and (e) m/e = 58 (propanal) following 2L propanal exposure on different surfaces.

trend for all adsorbates is Mo(110) > Co/Mo(110) > Ni/Mo(110). While in general the C−O bond length of the carbonyl group cannot be directly correlated with the binding strength, the DFT results in Tables 1 and 2 show that the C−O bond length trend is consistent with the binding energy trend for the η^2 configuration. For example, the clean Mo(110) surface shows the strongest binding energy and the largest C−O bond distance of the adsorbed $\eta^2(C,O)$-propanal, suggesting that the strong interaction between the carbonyl group and the Mo(110) surface weakens the C═O bond and likely makes its

dx.doi.org/10.1021/cs5012734 | ACS Catal. 2015, 5, 256−263

Table 3. Quantification of Propanal on Mo(110), NiMo(110), and CoMo(110) Surfaces[a]

	activity[b]				
surface	reforming	deoxygenation	ethylene formation	cecomposition	total
Mo(110)	0.000	0.032 (58.2)	0.000	0.023 (41.8)	0.055
NiMo(110)	0.011 (9.2)	0.000	0.064 (53.7)	0.044 (37.1)	0.119
CoMo(110)	0.064 (64.2)	0.000	0.000	0.036 (35.8)	0.099

[a]Selectivity percentages are shown in parentheses. [b]Molecule per metal atom.

scission more facile. This correlation between the C−O bond lengthening and the C−O bond scission is in agreement with those previously reported in the literature for furfural studies on NiFe[44] catalysts and Mo_2C[17] surfaces. Deposition of monolayers of Ni and Co on Mo(110) lowers the binding energies of the four adsorbates, suggesting potentially different reaction pathways from the pure Mo(110) surface. As has been demonstrated in many studies,[45] bimetallic surfaces often show binding energies and reaction pathways that are different from those of the parent metals. For instance, a previous DFT study of hydrogen and ethylene on Pd/Mo(110)[46] reported that the deposition of monolayer Pd reduces the binding energies in comparison to clean Mo(110). Since Ni and Pd are from the same group 10 metals, it could be expected that the binding energy trends of Ni/Mo(110) and Pd/Mo(110), in comparison to Mo(110), should be similar.

3.2. Reaction of Propanal on Mo(110), Ni/Mo(110), and Co/Mo(110). TPD experiments were performed on Mo(110), Ni/Mo(110), and Co/Mo(110) surfaces after exposure to 2L of propanal; the 2L exposure corresponded to a saturation of chemisorbed propanal. The desorbing gas-phase species included H_2 (m/e = 2), CO (m/e = 28), ethylene (m/e = 27), and propene (m/e = 41), as shown in Figure 2a−d, respectively. TPD spectra of propanal (m/e = 58) were also monitored and are shown in Figure 2e. No other reaction products were detected.

As shown in Figure 2a, hydrogen desorbs from Mo(110) at two maxima at 400 K (β_1) and 570 K (β_2). The peak desorption temperatures from Ni/Mo(110) and Co/Mo(110) are lower at 332 and 370 K, respectively. The relatively small hydrogen desorption peak at 570 K on Co/Mo(110) is likely from the uncovered surface sites of Mo(110). Previous TPD studies[47] reported that hydrogen, from the dissociation of H_2, desorbed from Mo(110) and ML Ni/Mo(110) at 370 and 280 K, respectively. Such a comparison indicates that hydrogen desorption from both Mo(110) and ML Ni/Mo(110) in the current study is reaction-limited from the decomposition of propanal.

For the Mo(110) surface, desorption peaks are observed at 268 and 445 K for m/e = 27, 28, and 58, which are from the cracking patterns of propanal. This has been confirmed on the basis of the relative mass spectrometer sensitivities for these peaks and also by the similar desorption temperatures and peak shapes, as shown in the Supporting Information. Because the intensity of the m/e = 28 peak for Mo(110) is consistent with the propanal cracking pattern, CO is not produced from the reaction of propanal on Mo(110). The dominant desorption product is propene (m/e = 41) at 510 K, suggesting deoxygenation pathway of propanal on clean Mo(110).

On ML Ni/Mo(110), propanal cracking pattern contributions to m/e = 28 are convoluted as shoulder peaks at 268 and 445 K. The desorption peak at 322 K is due to the cracking pattern of ethylene, since it is also observed at m/e = 27, while the peak at 368 K is from CO desorption. Overall, the reaction of propanal on Ni/Mo(110) produces both ethylene at 322 K and CO at 368 K. For the ML Co/Mo(110), CO desorbs at 368 K and appears to be the only carbon-containing product. Ethylene is not produced from this surface because the peaks at 268 and 445 K at m/e = 27 are from the cracking pattern of propanal. Propene is not observed from either Ni/Mo(110) or Co/Mo(110).

Possible reaction pathways of propanal on the three surfaces can then be summarized as follows: a reforming reaction involves the C═O bond retention to produce CO and H_2 via C−H and C−C bond scission, a decarbonylation reaction occurs via C−CO bond scission to produce ethylene and CO, a deoxygenation reaction produces propene through selective C═O bond cleavage, and total decomposition occurs via complete dissociation of all bonds to produce adsorbed atomic carbon, oxygen and hydrogen.

$$a\mathrm{CH_3CH_2CHO} \rightarrow a\mathrm{CO} + 3a\mathrm{H_2} + 2a\mathrm{C_{ad}} \quad (1)$$

$$b\mathrm{CH_3CH_2CHO} \rightarrow b\mathrm{C_2H_4} + b\mathrm{CO} + b\mathrm{H_2} \quad (2)$$

$$c\mathrm{CH_3CH_2CHO} \rightarrow c\mathrm{C_3H_6} + c\mathrm{O_{ad}} \quad (3)$$

$$d\mathrm{CH_3CH_2CHO} \rightarrow 3d\mathrm{C_{ad}} + d\mathrm{O_{ad}} + 3d\mathrm{H_2} \quad (4)$$

$$\mathrm{CO\ yield} = a + b \Rightarrow a = \mathrm{CO\ yield} - b \quad (5)$$

$$\mathrm{C_2H_4\ yield} = b \Rightarrow b = \mathrm{C_2H_4\ yield} \quad (6)$$

$$\mathrm{C_3H_6\ yield} = c \Rightarrow c = \mathrm{C_3H_6\ yield} \quad (7)$$

$$\mathrm{H_2\ yield} = 3a + b + 3d \Rightarrow d = (\mathrm{H_2\ yield} - 3a - b)/3 \quad (8)$$

As shown in the equations above, the activities of four reactions, a−d, represent the stoichiometric amount of chemisorbed propanal (molecule per metal atom) undergoing each reaction pathway. Reactivity quantification is performed on the basis of the procedures shown in the Supporting Information, modified from the previously described method,[43] since there is no saturation coverage of CO on Mo(110) in the literature, and the results are summarized in Table 3.

TPD quantification suggests that a majority of propanal undergoes the deoxygenation reaction and the rest undergoes total decomposition on Mo(110). The reaction pathways are significantly altered on Ni/Mo(110), which shows an increased activity for reforming and total decomposition. In addition, the ML Ni/Mo(110) surface shows a high activity for ethylene production. Reforming activity is even higher on Co/Mo(110), with the rest undergoing total decomposition. It should be pointed out that although the CO peak area is larger on Ni/Mo(110) than on Co/Mo(110) in Figure 2b, after taking mass balance into account as shown in eq 5, our quantification results indicate a higher reforming activity on Co/Mo(110). In other words, since CO is produced from both reforming and decarbonylation reactions, Ni/Mo(110) shows a smaller reforming activity due to its high ethylene yield. Overall, the

dx.doi.org/10.1021/cs5012734 | ACS Catal. 2015, 5, 256−263

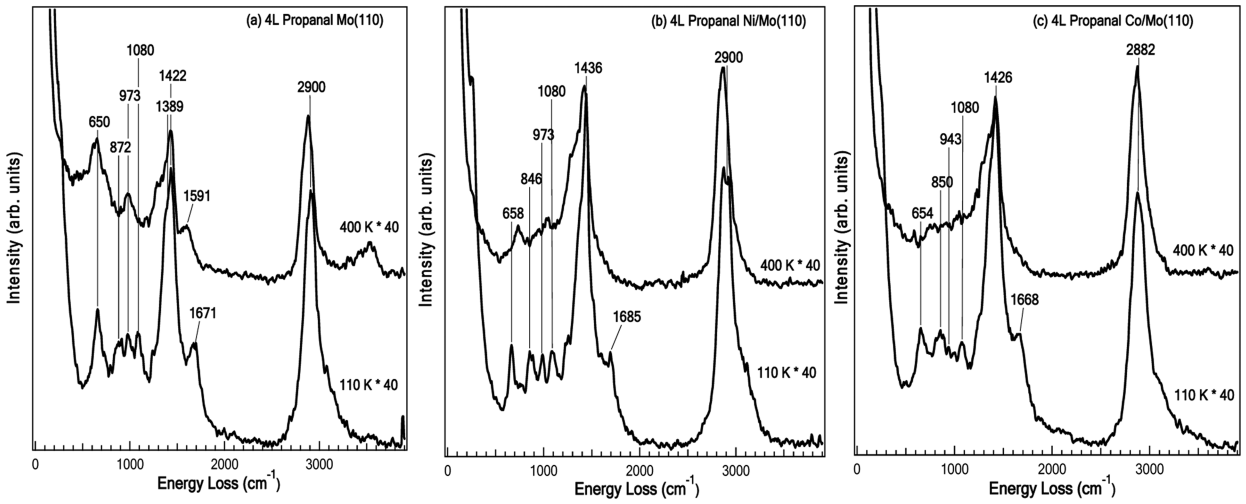

Figure 3. HREEL spectra of 4L propanal on (a) Mo(110), (b) ML Ni/Mo(110), and (c) ML Co/Mo(110).

highest activity is observed for deoxygenation via C═O bond scission on Mo(110), decarbonylation to produce ethylene via C−C bond scission on Ni/Mo(110), and reforming to produce syngas via C−C and C−H bond scission on Co/Mo(110).

HREELS experiments were performed to determine the surface reaction intermediates. The HREEL spectra of 4L propanal on Mo(110), ML Ni/Mo(110), and ML Co/Mo(110) surfaces at 110 and 400 K are shown in parts a−c of Figure 3, respectively. The vibrational features of propanal observed at 110 K on Mo(110) are summarized in Table 4,

Table 4. Vibrational Assignment of Propanal in cm^{-1}

assignment type of mode	infrared[48]	calcd on Mo(110)[a]	Mo(110) 110 K[b]
$\nu(CH_3)$	2966	2968	2900
$\nu(CH_2)$	2909	2968	2900
$\nu(CO)$	1730		1671
$\delta(CH_2)$	1458	1441	1422
$\delta(CH_3)$	1418	1355	1389
$\nu_a(CCC)$	1092, 1120	1089	1080
$\rho(CH_3)$	898	973	973
$\delta(CCO)$	660	592	650

[a]Calculated using DFT. [b]This work.

along with the DFT-calculated frequencies of propanal on Mo(110). The main vibrational features are as follows: $\delta(CCO)$, 650 cm^{-1}; $\rho(CH_3)$, 973 cm^{-1}; $\nu_a(CCC)$, 1080 cm^{-1}; $\delta(CH_3)$, 1389 cm^{-1}; $\delta(CH_2)$, 1422 cm^{-1}; $\nu(CO)$, 1671 cm^{-1}; $\nu(CH_2)$, 2900 cm^{-1}; $\nu(CH_3)$, 2900 cm^{-1}. The observation of these characteristic vibrational modes indicates that propanal adsorbs molecularly on Mo(110) at 110 K. After the surface is heated to 400 K, the $\nu(CO)$ mode at 1671 cm^{-1} shifts to a lower frequency and becomes broader and the intensity is reduced, suggesting that the carbonyl group interacts with the Mo(110) surface to form an $\eta^2(C,O)$-propanal surface intermediate, in agreement with the DFT prediction shown in Figure 1a. In addition, the presence of most of the skeletal vibrational modes at 400 K suggests that the $\eta^2(C,O)$-propanal species is still stable at 400 K, consistent with the TPD result, which shows that propene production occurs at temperatures higher than 400 K.

Similar to the case for Mo(110), propanal adsorbs molecularly on both ML Ni/Mo(110) and ML Co/Mo(110) at 110 K, as indicated in Figure 3b and c. When the surface is heated to 400 K, however, the $\delta(CCO)$ mode at around 650 cm^{-1} and the $\nu_a(CCC)$ mode at 1080 cm^{-1} disappear from both surfaces, indicating that the skeletal structure of propanal disappears and the C−C bond scission has already occurred. In fact, the $\nu(CO)$ mode also disappears and only modes associated with the surface hydrocarbon fragments remained. This is in agreement with the TPD results, which show the desorption of C−C bond scission products between 200 and 400 K.

The major difference between the HREEL spectra of propanal on Mo(110) and those on bimetallic surfaces is that the decomposition of C−C−C and C═O on Mo(110) does not start until 400 K, whereas on the bimetallic surfaces the decomposition of the C−C−C bond is already complete by 400 K.

3.3. Reaction of 1-Propanol on Mo(110), Ni/Mo(110), and Co/Mo(110). The reaction of 1-propanol on Mo(110)[36] and Co/Mo(110)[32] has been studied via TPD and HREELS by Friend et al. Since our focus is to compare the bond scission activities of Mo(110) and metal-modified Mo(110) surfaces, particularly the difference between the C═O bond of aldehyde and the C−O bond of alcohol under the same reaction

Table 5. Quantification of 1-Propanol on Mo(110), NiMo(110), and CoMo(110) Surfaces[a]

	activity[b]						
surface	reforming	deoxygenation	ethylene formation	propanal formation	propane formation	decomposition	total
Mo(110)	0.000	0.054 (65.9)	0.000	0.010 (12.2)	0.004 (4.9)	0.014 (17.1)	0.082
NiMo(110)	0.027 (36.0)	0.000	0.039 (52.0)	0.007 (9.3)	0.000	0.002 (2.7)	0.075
CoMo(110)	0.086 (55.8)	0.000	0.055 (35.7)	0.003 (1.9)	0.000	0.010 (6.5)	0.154

[a]Selectivity percentages are shown in parentheses. [b]Molecule per metal atom.

dx.doi.org/10.1021/cs5012734 | ACS Catal. 2015, 5, 256−263

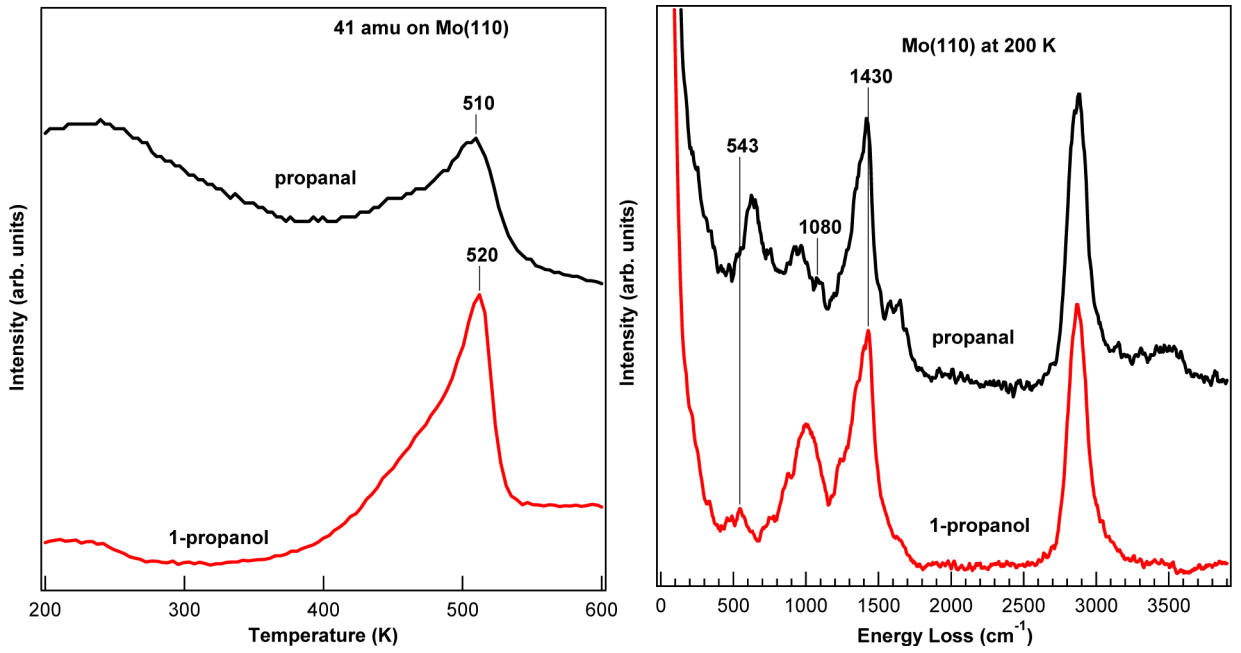

Figure 4. Comparison of propene (m/e = 41) formation and surface intermediates on Mo(110) at 400 K from propanal and 1-propanol.

conditions, here we will summarize our results for the reactions of 1-propanol for comparison. The TPD and HREELS results of 1-propanol on all three surfaces, vibrational assignments at 110 K, and the DFT frequency calculations for 1-propanol on Mo(110) are provided in the Supporting Information.

The reaction activity of 1-propanol on all three surfaces is summarized in Table 5. In summary, 1-propanol on Mo(110) undergoes mainly deoxygenation via C−O bond scission, with trace amounts undergoing dehydrogenation to form propanal, and propane, and total decomposition to produce surface carbon, oxygen, and hydrogen. The deoxygenation product, propene, is no longer present upon bimetallic modification. On both bimetallic surfaces, reforming activity is enhanced and, in addition to syngas, ethylene and propanal are also observed via decarbonylation and dehydrogenation. As shown in the Supporting Information, HREEL results reveal that 1-propanol adsorbs molecularly at 110 K on all surfaces and decomposition occurs via the 1-propoxy surface intermediate from the O−H bond scission. The main difference between Mo(110) and bimetallic surfaces is that C−O bond scission on Mo(110) starts around 400 K, whereas the C−C bond cleavage has begun at 200 K for a fraction of the 1-propoxide surface species on both Ni/Mo(110) and Co/Mo(110) and is complete by 400 K. Similar to the case for propanal, the highest selectivities are observed for deoxygenation, decarbonylation, and reforming on Mo(110), ML Ni/Mo(110), and ML Co/Mo(110), respectively. Overall, the results for 1-propanol on Mo(110) and Co/Mo(110) are consistent with those reported by Friend et al.[36,32]

4. DISCUSSION

DFT results show that the binding energies of propanal and 1-propanol on Mo(110) can be reduced by the deposition of surface monolayers of Ni and Co, and that the binding energy trend is Mo(110) > Co/Mo(110) > Ni/Mo(110). HREELS results show that on all three surfaces both 1-propanol and propanal adsorb molecularly at 110 K. TPD results confirm that the major reaction pathways for propanal and 1-propanol are also similar: Mo(110) selectively cleaves the C−O/C═O bond to produce propene and shows the highest activity for deoxygenation; Ni/Mo(110) and Co/Mo(110) show an enhanced activity in the C−C and C−H bond scission.

The combination of TPD and HREELS measurements provide further insights into the reaction pathways of propanal and 1-propanol. For example, as compared in Figure 4, the observation of similar propene desorption temperatures and peak shapes suggests that Mo(110) is active for both C═O and C−O bond scission and that the decomposition pathways are similar for propanal and 1-propanol. This is consistent with the HREELS results, which show the presence of similar types of surface intermediates that contain the C−C−C−O skeletal structure at 400 K on Mo(110), $\eta^2(C,O)$-propanal, and 1-propoxide, as shown in Figure 4. In comparison to the bimetallic surfaces, Mo(110) is less active toward C−C bond cleavage, leading to the selective C═O/C−O scission at 400 K.

In contrast, the deoxygenation reaction is no longer present on bimetallic surfaces, which favor the C−C and C−H bond scission to produce CO and H_2. The absence of propene formation in TPD (Figure 2 and Figure S2, Supporting Information) is consistent with the HREELS results (Figure 3 and Figure S3, Supporting Information) of the dissociation of the C−C−C−O skeletal structure. The primary difference between the two bimetallic surfaces is that, for both oxygenates, the reforming activity on Co/Mo(110) is larger than that on Ni/Mo(110). This is consistent with previous results which show that a bimetallic surface with higher oxygenate binding energies possesses a higher reforming activity.[49]

The ML Ni/Mo(110) surface also shows the decarbonylation pathway to produce ethylene and CO. For propanal, ethylene is observed only on ML Ni/Mo(110), while for 1-propanol ethylene is observed on both Ni/Mo(110) and Co/Mo(110). It is worth noting, however, that Ni/Mo(110) consistently shows the highest selectivity toward ethylene production for both molecules.

Such differences in reactivity can be related to the binding strength. For example, propanal shows the largest binding

dx.doi.org/10.1021/cs5012734 | ACS Catal. 2015, 5, 256−263

energy on Mo(110), indicating a strong interaction between the carbonyl group and the surface, stabilizing the adsorbed $\eta^2(C,O)$-propanal surface intermediate. In addition, the length of the C═O bond in adsorbed propanal on Mo(110) has also increased significantly, in comparison to that of molecular propanal, making C═O bond scission more facile. Previous studies of hydrodeoxygenation reactions of furfural on NiFe bimetallic catalyst[44] and Mo_2C[17] also show a correlation between the C−O bond lengthening due to stronger binding of the carbonyl group on the catalytic surface and the C−O bond scission. On the other hand, the lower binding energies of oxygenates on the bimetallic surfaces should be responsible for retaining the C−O/C═O bond, leading to an enhanced selectivity toward C−C and C−H bond scission.

Furthermore, decomposition reaction studies of 2-propanol on Mo(110) and Co/Mo(110)[30] have previously suggested that the difference in reaction pathways can be attributed to the difference in the metal−oxygen bond strengths. Calculations for oxygen binding energy (OBE) in Table S1 in the Supporting Information showed that the OBE follows a trend similar to those of propanal and 1-propanol, where the binding energy is reduced upon bimetallic modifications, supporting the previous claim that a stronger Mo−O binding energy results in breaking the C−O bond due to a stronger thermodynamic driving force. It should be pointed out that under catalytic reaction conditions Mo and its bimetallic surfaces might be in the form of carbides and oxides.[50] The trend in the current study on metal-modified Mo(110) is similar to a previous study of a C2 oxygenate, ethylene glycol, on Mo_2C and Ni-modified Mo_2C surfaces.[51] For example, results from that study revealed that the unmodified Mo_2C surface favored the C−O bond scission, while ML Ni/Mo_2C was selective toward the C−C bond cleavage due to strong atomic carbon and oxygen binding energies on Mo_2C.[51] The similar trends between the two studies suggest that results from the current paper should have relevance to Mo-based bimetallic catalysts.

Our current studies not only confirm the importance of the binding strength of oxygen and C3 oxygenates in determining the reaction pathways but also shed light on the use of nonprecious bimetallic surfaces to control bond scission. We hope our experimental observations would inspire further detailed DFT calculations to explain the role of Ni and Co admetals and how they change the electronic structures and subsequently the reaction network and activation barriers.

5. CONCLUSIONS

Results from this investigation provide insight into how the C−O/C═O, C−C, and C−H bond scission can be controlled by surface modification of Mo(110) with Ni and Co. The reactions of propanal and 1-propanol are compared on Mo(110), ML Ni/Mo(110), and ML Co/Mo(110) via DFT and parallel TPD and HREELS experiments. DFT results predict that the binding energies of 1-propanol, propanal, 1-propoxy, and propionyl can be reduced by the modification of Mo(110) with Ni and Co admetals which shows the trend Mo(110) > Co/Mo(110) > Ni/Mo(110). For both propanal and 1-propanol, a highly selective deoxygenation activity is observed on Mo(110) via the C═O/C−O bond cleavage to form propene, although a small amount undergoes total decomposition. Deposition of a monolayer of Ni and Co on the Mo(110) surface enhances the C−C and C−H bond scission. The Co/Mo(110) surface shows the highest selectivity for reforming to produce CO and H_2, while the Ni/Mo(110) surface shows the highest selectivity for decarbonylation to produce ethylene and CO.

■ ASSOCIATED CONTENT

Supporting Information

The following file is available free of charge on the ACS Publications website at DOI: 10.1021/cs5012734.

Additional details of the calculations and characterization data (PDF)

■ AUTHOR INFORMATION

Corresponding Author

*J.G.C.: tel, (212) 854-6166; fax, (212) 854-3054; e-mail, jgchen@columbia.edu.

Notes

The authors declare no competing financial interest.

■ ACKNOWLEDGMENTS

This work was supported as part of the Catalysis Center for Energy Innovation, an Energy Frontier Research Center funded by the U.S. Department of Energy, Office of Basic Energy Sciences, Office of Science, under Award Number DE-SC0001004. The DFT calculations in this work were performed using computational resources at the Center for Functional Nanomaterials, Brookhaven National Laboratory, supported by the U.S. DOE/BES, under Contract No. DE-AC02-98CH10886.

■ REFERENCES

(1) Laskar, D. D.; Yang, B.; Wang, H.; Lee, J. *Biofuels, Bioprod. Biorefin.* **2013**, *7*, 602−626.
(2) Zhou, C.-H.; Xia, X.; Lin, C.-X.; Tong, D.-S.; Beltramini, J. *Chem. Soc. Rev.* **2011**, *40*, 5588−5617.
(3) Medlin, J. W. *ACS Catal.* **2011**, *1*, 1284−1297.
(4) Mavrikakis, M.; Barteau, M. A. *J. Mol. Catal. A: Chem.* **1998**, *131*, 135−147.
(5) Zacher, A. H.; Olarte, M. V.; Santosa, D. M.; Elliott, D. C.; Jones, S. B. *Green Chem.* **2014**, *16*, 491−515.
(6) Furimsky, E. *Appl. Catal., A* **2000**, *199*, 147−190.
(7) Gosselink, R. W.; Hollak, S. A. W.; Chang, S.-W.; van Haveren, J.; de Jong, K. P.; Bitter, J. H.; van Es, D. S. *ChemSusChem* **2013**, *6*, 1576−1594.
(8) Alonso, D. M.; Wettstein, S. G.; Dumesic, J. A. *Chem. Soc. Rev.* **2012**, *41*, 8075−8098.
(9) Yu, W.; Porosoff, M. D.; Chen, J. G. *Chem. Rev.* **2012**, *112*, 5780−5817.
(10) Runnebaum, R. C.; Nimmanwudipong, T.; Block, D. E.; Gates, B. C. *Catal. Sci. Technol.* **2012**, *2*, 113−118.
(11) Kim, S. M.; Lee, M. E.; Choi, J.-W.; Suh, D. J.; Suh, Y.-W. *Catal. Commun.* **2011**, *16*, 108−113.
(12) Zhao, C.; Kou, Y.; Lemonidou, A. A.; Li, X.; Lercher, J. A. *Angew. Chem.* **2009**, *121*, 4047−4050.
(13) Yang, Y.; Ochoa-Hernández, C.; de la Peña O'Shea, V. A.; Coronado, J. M.; Serrano, D. P. *ACS Catal.* **2012**, *2*, 592−598.
(14) Davda, R. R.; Shabaker, J. W.; Huber, G. W.; Cortright, R. D.; Dumesic, J. A. *Appl. Catal., B* **2003**, *43*, 13−26.
(15) Ren, H.; Yu, W.; Salciccioli, M.; Chen, Y.; Huang, Y.; Xiong, K.; Vlachos, D. G.; Chen, J. G. *ChemSusChem* **2013**, *6*, 798−801.
(16) Prasomsri, T.; Nimmanwudipong, T.; Roman-Leshkov, Y. *Energy Environ. Sci.* **2013**, *6*, 1732−1738.
(17) Xiong, K.; Lee, W.-S.; Bhan, A.; Chen, J. G. *ChemSusChem* **2014**, *7*, 2146−2149.
(18) Kelly, T. G.; Chen, J. G. *Green Chem.* **2014**, *16*, 777−784.
(19) Sousa, L. A.; Zotin, J. L.; Teixeira da Silva, V. *Appl. Catal., A* **2012**, *449*, 105−111.

(20) Boullosa-Eiras, S.; Lødeng, R.; Bergem, H.; Stöcker, M.; Hannevold, L.; Blekkan, E. A. *Catal. Today* **2014**, *223*, 44−53.
(21) Lee, W.-S.; Wang, Z.; Wu, R. J.; Bhan, A. *J. Catal.* **2014**, *319*, 44−53.
(22) Chen, X.; Zhang, T.; Ying, P.; Zheng, M.; Wu, W.; Xia, L.; Li, T.; Wang, X.; Li, C. *Chem. Commun.* **2002**, 288−289.
(23) Jian-Wei, H.; Kuhn, W. K.; Goodman, D. W. *Surf. Sci.* **1993**, *292*, 248−260.
(24) Gerlach, A.; Maurice, V.; Marcus, P. *Surf. Sci.* **1996**, *352*−*354*, 9−14.
(25) Murphy, S.; Usov, V.; Shvets, I. V. *Surf. Sci.* **2007**, *601*, 5576−5584.
(26) Bauer, E. *J. Phys.-Condens. Matter* **1999**, *11*, 9365−9385.
(27) Mikkelsen, A.; Ouattara, L.; Lundgren, E. *Surf. Sci.* **2004**, *557*, 109−118.
(28) Tikhov, M.; Bauer, E. *Surf. Sci.* **1990**, *232*, 73−91.
(29) Jian-Wei, H.; Goodman, D. W. *Surf. Sci.* **1991**, *245*, 29−40.
(30) Chen, D. A.; Friend, C. M. *J. Phys. Chem.* **1996**, *100*, 17640−17647.
(31) Chen, D. A.; Friend, C. M. *J. Phys. Chem. B* **1997**, *101*, 5712−5716.
(32) Chen, D. A.; Friend, C. M. *Langmuir* **1998**, *14*, 1451−1457.
(33) Chen, D. A.; Friend, C. M. *J. Am. Chem. Soc.* **1998**, *120*, 5017−5023.
(34) Queeney, K. T.; Friend, C. M. *J. Phys. Chem. B* **1998**, *102*, 5178−5181.
(35) Friend, C. M.; Xu, X. *Annu. Rev. Phys. Chem.* **1991**, *42*, 251−278.
(36) Wiegand, B. C.; Uvdal, P.; Serafin, J. G.; Friend, C. M. *J. Phys. Chem.* **1992**, *96*, 5063−5069.
(37) Deiner, L. J.; Friend, C. M. *Surf. Sci.* **2003**, *539*, 21−30.
(38) Mei, D.; Karim, A. M.; Wang, Y. *ACS Catal.* **2012**, *2*, 468−478.
(39) Queeney, K. T.; Arumainayagam, C. R.; Balaji, A.; Friend, C. M. *Surf. Sci.* **1998**, *418*, L31−L38.
(40) Kresse, G.; Hafner, J. *Phys. Rev. B: Condens. Matter Mater. Phys.* **1993**, *48*, 13115−13118.
(41) Kresse, G.; Furthmuller, J. *Phys. Rev. B: Condens. Matter Mater. Phys.* **1996**, *54*, 11169−11186.
(42) Kresse, G.; Furthmüller, J. *Comput. Mater. Sci.* **1996**, *6*, 15−50.
(43) Myint, M.; Yan, Y.; Chen, J. G. *J. Phys. Chem. C* **2014**, *118*, 11340−11349.
(44) Sitthisa, S.; An, W.; Resasco, D. E. *J. Catal.* **2011**, *284*, 90−101.
(45) Chen, J. G.; Menning, C. A.; Zellner, M. B. *Surf. Sci. Rep.* **2008**, *63*, 201−254.
(46) Zellner, M. B.; Goda, A. M.; Skoplyak, O.; Barteau, M. A.; Chen, J. G. *Surf. Sci.* **2005**, *583*, 281−296.
(47) Sheng, W.; Bivens, A. P.; Myint, M.; Zhuang, Z.; Forest, R. V.; Fang, Q.; Chen, J. G.; Yan, Y. *Energy Environ. Sci.* **2014**, *7*, 1719−1724.
(48) Sbrana, G.; Schettino, V. *J. Mol. Spectrosc.* **1970**, *33*, 100−108.
(49) Yu, W.; Barteau, M. A.; Chen, J. G. *J. Am. Chem. Soc.* **2011**, *133*, 20528−20535.
(50) Porosoff, M. D.; Yang, X.; Boscoboinik, J. A.; Chen, J. G. *Angew. Chem., Int. Ed.* **2014**, *53*, 6705−6709.
(51) Yu, W.; Salciccioli, M.; Xiong, K.; Barteau, M. A.; Vlachos, D. G.; Chen, J. G. *ACS Catal.* **2014**, *4*, 1409−1418.